Supplementary Information

1   Microfluidic chip design

1.1   Design layers

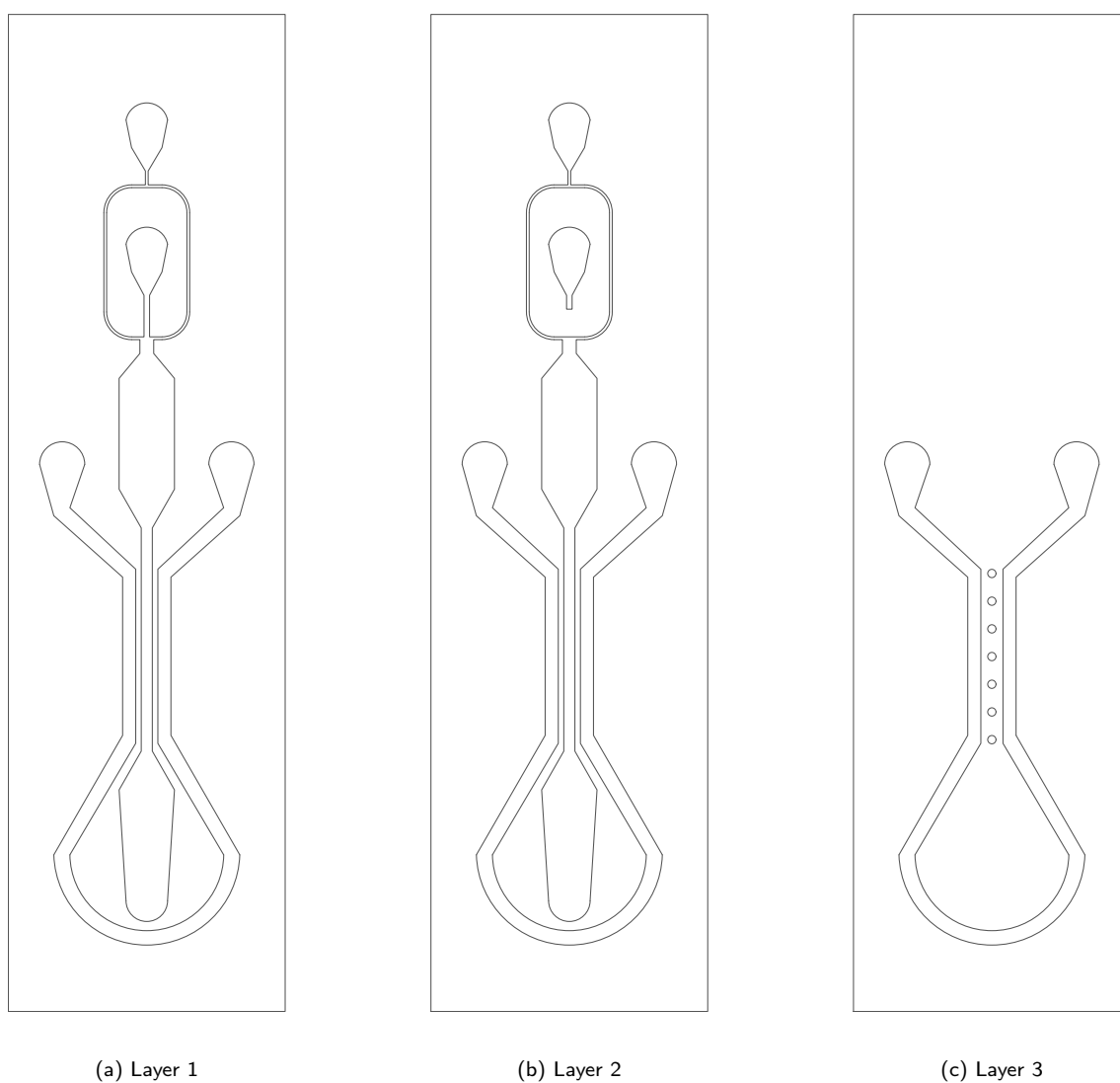(a) Layer 1   (b) Layer 2   (c) Layer 3

Fig. 1 Scale drawings of the 3 design layers used for micro-fabrication. The 3D microfluidic device requires the manufacturing of a multi-layer mold. The first and second layer are almost identical, with the exception of a 1000 μm-long segment downstream of the dispersed phase (aqueous solution) inlet. The consecutive exposure of the first two layers results in differential channel height on this segment, necessary for step-emulsification (see figure 2). The third and last layer allows the exposure of the cylindrical wells above the rheological secion of the main channel. The lateral channel is exposed at every layer and thus spans the full height of the chip, optimizing air flow. *(Scale: each drawing is outlined by a 36x10 mm rectangle)*
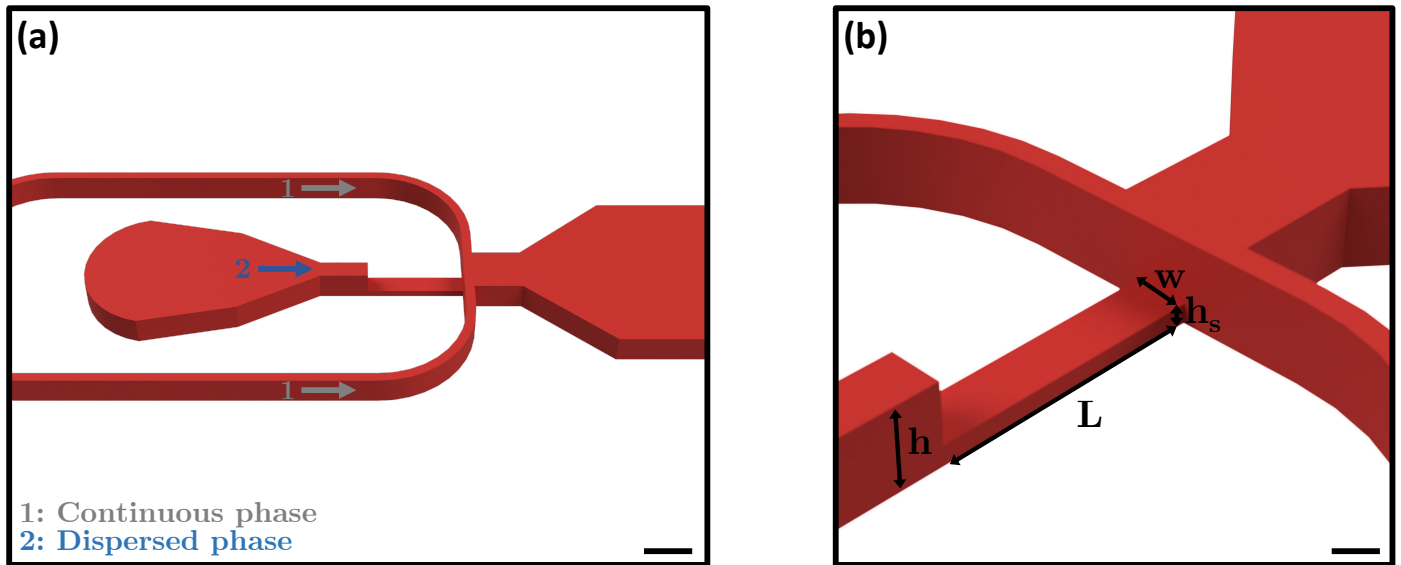
1.2 Step-emulsification dropmaker

Fig. 2 Detailed views of the step-emulsification dropmaker. (a) A narrowing of the dispersed phase (water, 2) inlet produces a variation in confinement geometry, leading to emulsification when the dispersed phase flow meets the continuous phase (fluorinated oil, 1) flow. (Scale bar: 500 µm) (b) Dimensions of the narrowed section. The dispersed phase inlet has a $w = 300$ µm width and a $h \in [200, 300]$ µm height, depending on the height of the spin-coated SU-8 layers. The step has a $L = 1000$ µm length and a $h_s = h/4$ height. (Scale bar: 300 µm)
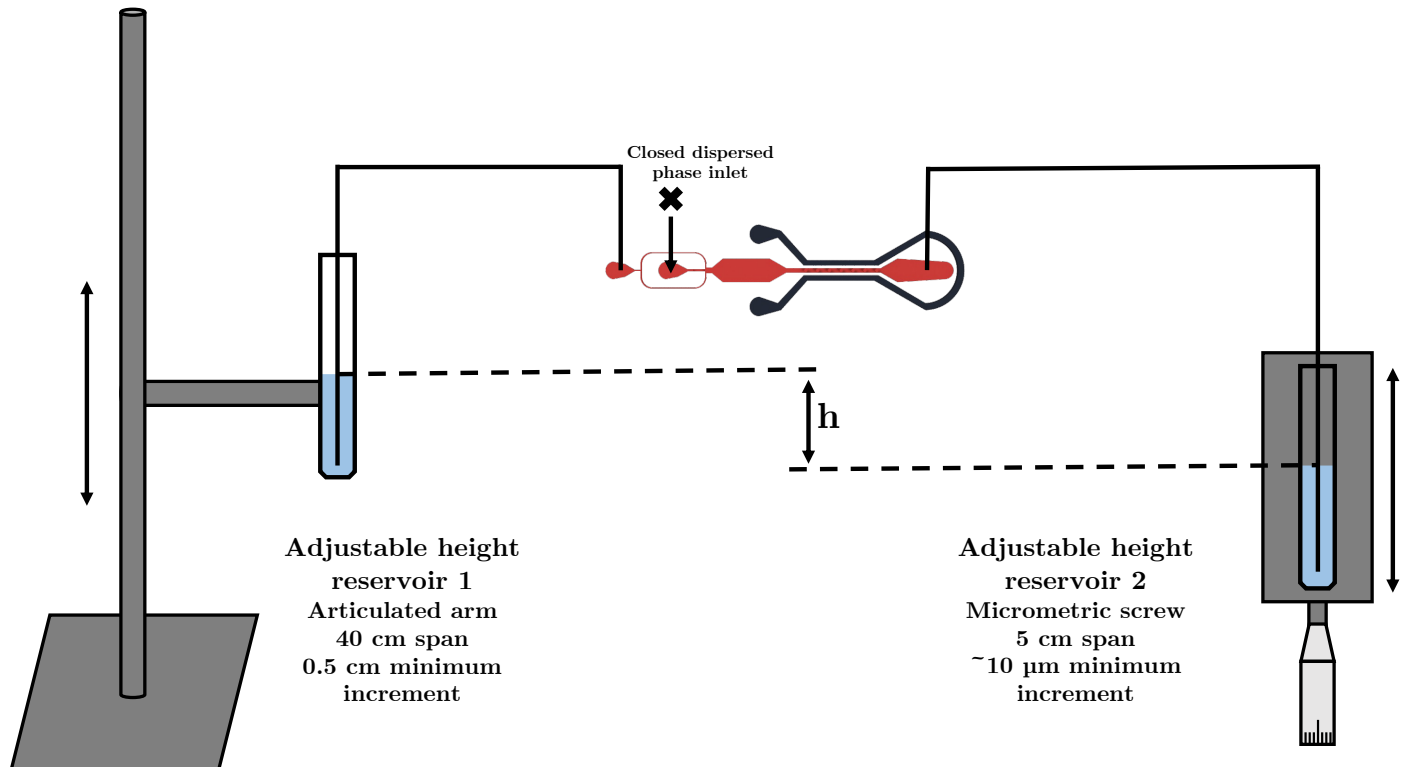
2 Flow control setup

Fig. 3 Gravitationnal flow control setup. After droplet production, the dispersed phase inlet is closed and the continuous phase inlet is switched from a syringe pump to a fluorinated oil reservoir. The outlet is also connected to a similar reservoir. Control of the differential height h between the two reservoirs adjusts the differential pressure $\Delta P = \rho g h$, allowing flow control precise enough to enable droplet loading and residual flow balancing.

3 Error on droplet volume measurement

To monitor solute concentration during the shrinking process, our approach relies on precise measurement of the droplet's volume, based on brightfield microscopy images of the droplet. The automated approach we developed used software autofocus to ensure focus is made on the droplet's edge at the equatorial plane throughout the shrinking process. Post-experiment, edge detection is performed via circular Hough transform, and the measured radius is used to compute droplet volume, assuming the droplet is spherical. To evaluate the incertainty linked with our volume measurement method, we discuss the error linked with each of its steps, as well as the validity of the droplet sphericity assumption.

3.1 Autofocus

Software autofocus is performed by the ZEN Blue Software (Zeiss). Repeated autofocus attempts on a given droplet allowed us to verify the precision of the method, with focus measurement at ± 200 nm, compared to a $\pm 2.5\ \mu$m precision for manual focus in similar conditions. Furthermore, droplet edge detection proved to be quite tolerant to focus errors, with a $\pm 5\ \mu$m focus error resulting in a 0.4% error on radius, equivalent to a 1.2% error on volume. With the use of autofocus, we estimate the error on droplet volume measurement to be $\delta_V^f < 1\%$.

3.2 Edge detection

Circular Hough transform is used to detect the edge of the droplet. On a given image, this algorithm detects the external edge of circles standing out from the background. On brightfield microscopy images, the edge of the droplet, the interface between the droplet and the continuous phase is materialized by a darker strip. The Hough transform algorithm places the edge of the droplet at the point of maximum contrast between the bright background and this darker strip. Using optical path numerical simulations[1], we verified that the localization of the detected edge corresponds to the actual droplet edge with an error $< \lambda$, the wavelength of the incident light. As the error on edge detection is absolute, its impact on volume detection depends on droplet radius. In table 1 are listed the maximum relative errors on measured radius and volume for droplet of various sizes.

Droplet radius	150 μm	100 μm	50 μm	20 μm
Relative error on measured radius	0.3%	0.5%	1%	2.5%
Relative error on measured volume (δ_V^e)	1%	1.5%	3%	7.5%

Table 1 Maximum relative error on droplet radius and volume linked with a λ error on edge detection, for droplets between 150 μm and 20 μm in radius

3.3 Droplet sphericity

To compute droplet volume from the measured radius, we rely on the assumption that the droplet is spherical, and that its volume can be calculated as $V = \frac{4}{3}\pi R^3$. Droplet shape depends on the surface tension between its content (water in our case) and the surrounding continuous phase. We measured a $\gamma_{0.2} \approx 5$ mN.m^{-2} between water and fluorinated oil with RAN-008 fluorosurfactant at a 0.2% w/w concentration. We used numerical simulations based on the resolution of the Gauss-Laplace equation[2] to compute the profile of the droplet and estimate the error on volume measurement caused by its non-sphericity. For droplets of 150 μm radius, the maximum allowed in our device, the error is $\delta_V^s < 1\%$.

3.4 Maximum error on droplet volume measurement

The maximum error on droplet volume measurement can be estimated as $\delta_V = \delta_V^f + \delta_V^e + \delta_V^s$. For droplets above 40 μm in radius $\delta_V < 5\%$. For droplets under 40 μm in radius, error on edge detection increases, leading to $\delta_V < 10\%$.
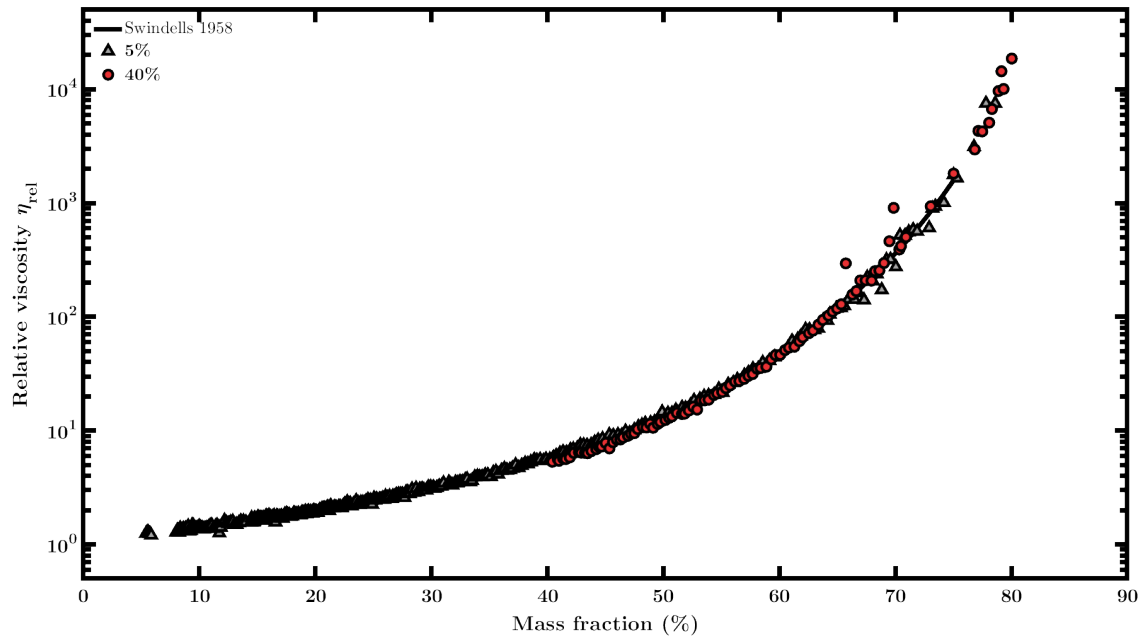
4   Viscosity of sucrose

Fig. 4 Relative viscosity as a function of mass fraction for aqueous sucrose solutions, comparing microrheology in shrinking droplet results (△) and tabulated data [3] (solid line). Two distinct experiments are reproduced here, with initial sucrose mass fraction of 5% and 40% respectively. The two points showing a clear deviation from the tabulated values have been correlated with the tracking of a fluorescent tracer dipole.
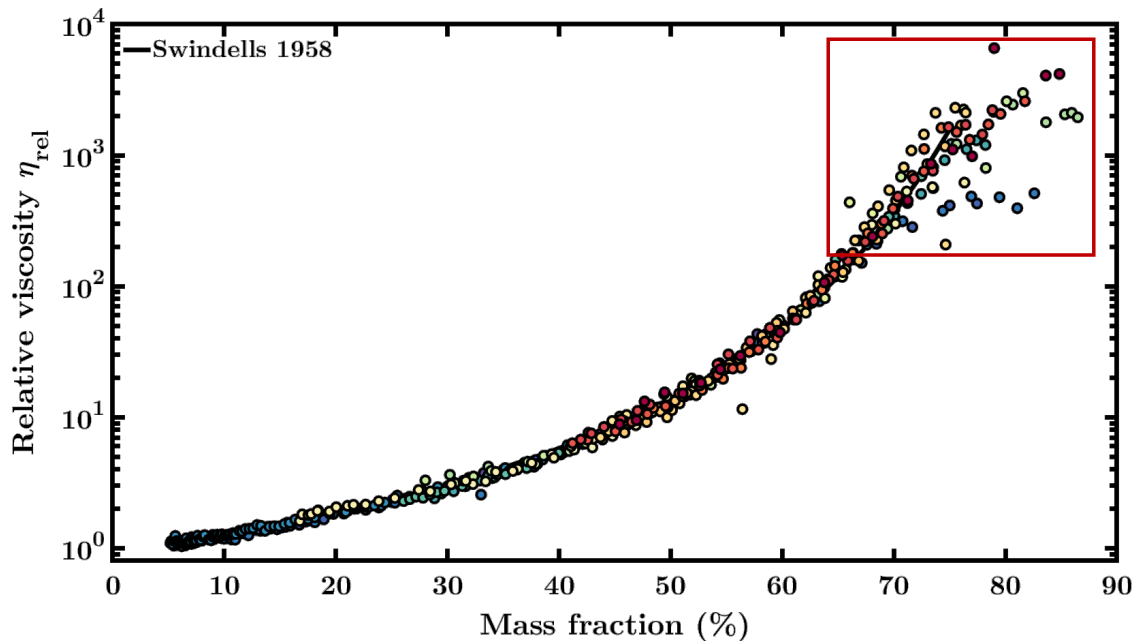

Fig. 5 Relative viscosity as a function of mass fraction for aqueous sucrose solutions, comparing microrheology in shrinking droplet results (○) and tabulated data [3] (solid line). Twenty distinct experiments are reproduced here, with initial sucrose mass fraction varying between 1% and 40%. For mass fraction above 70%, corresponding to viscosities above 200 mPa.s, some curves display a plateau behavior (highlighted by a red rectangle).

Notes and references

1 F. Gómez, R. Dutra, L. Pires, G. R. d. S. Araújo, B. Pontes, P. M. Neto, H. Nussenzveig and N. Viana, *Physical Review Applied*, 2021, **15**, 064012.

2 S. Zholob, A. Makievski, R. Miller and V. Fainerman, *Advances in Colloid and Interface Science*, 2007, **134–135**, 322–329.

3 J. F. Swindells, C. F. Snyder and R. C. Hardy, *National Bureau of Standards - United States Department Of Commerce*, 1958, 8.